Insulating materials for HVDC cable accessories: effects on the electric field in nonstationary situations

Gilbert Teyssedre, Thi Thu Nga Vu, Séverine Le Roy

▶ **To cite this version:**

Gilbert Teyssedre, Thi Thu Nga Vu, Séverine Le Roy. Insulating materials for HVDC cable accessories: effects on the electric field in nonstationary situations. IEEE Electrical Insulation Magazine, 2022, 38 (5), pp.6-17. ⟨10.1109/MEI.2022.9858038⟩. ⟨hal-03785931⟩

HAL Id: hal-03785931

https://hal.science/hal-03785931v1

Submitted on 23 Sep 2022

HAL is a multi-disciplinary open access archive for the deposit and dissemination of scientific research documents, whether they are published or not. The documents may come from teaching and research institutions in France or abroad, or from public or private research centers.

L'archive ouverte pluridisciplinaire **HAL**, est destinée au dépôt et à la diffusion de documents scientifiques de niveau recherche, publiés ou non, émanant des établissements d'enseignement et de recherche français ou étrangers, des laboratoires publics ou privés.

HAL Authorization

Insulating materials for HVDC cable accessories: impact on the electric field in non-stationary situations

Gilbert Teyssedre[1*], Thi Thu Nga Vu[2], Séverine Le Roy[1]

[1] Laplace, University of Toulouse and CNRS, Toulouse, France
[2] Electric Power University, Hanoi, Vietnam
*gilbert.teyssedre@laplace.univ-tlse.fr

Cite as: G. Teyssedre, T.T.N. Vu, S. Le Roy, "*Insulating materials for HVDC cable accessories: impact on the electric field in non-stationary situations*", **IEEE Electr. Insul. Mag.** Vol. 38, n°5, pp. 6-17, **2022**

***Abstract*—With the move to DC technologies for power transmission, the computation of the field distribution in insulations has become a tricky task as the materials response is less well mastered as under ac stress. This is true for HVDC cables where essentially the conductivity law must be identified for the used insulating material. Cables represent a relatively simple case study. Accessories as cable joints and terminations are certainly more delicate to address. First, more than one material has to be handled; second the translational symmetry is broken, and tangential fields have to be computed in a situation of inhomogeneous temperature conditions. Finally, non-stationary situations have to be managed and modelled for accounting for on-line operations as well as surges seen by cables. Our purpose in this work is to give an overview on how far these transient phenomena are handled in the literature and to demonstrate how far the electrical as well as thermal properties of materials actually determine the field distributions.**

Keywords—HVDC cable joints, field distribution, FEM simulation, XLPE

Introduction

HVDC technologies are definitively adopted today, boosted by needs in increasing power supply and in a favorable context of renewable energy sources. The later imposes constrains on energy production localization, and requires consolidation of the network and realization of new interconnections due to the intermittence of production and consumption, hence the variability in transmission fluxes. German corridors, hundreds of km long, are already on realization with 525kV HVDC land cables [**1**]. The question is therefore not whether HVDC will emerge, but rather in which voltage range: down to distribution scale or medium voltage? Up to extra-high voltage with the concept of intercontinental network [**2**]? and at which development speed. As part of this network evolution requires new lines, the trends for improving acceptability and fastening the decision-to-installation period is to develop cable solutions, which are elsewhere necessary for offshore energy production. HVAC technologies are mature for long, cable solutions are available for very high voltages albeit the length is limited by the need to compensate the capacitive current. Moving to HVDC may not represent at first sight a big challenge as broadly speaking the breakdown strength of insulations is greater for DC stress than for AC. Besides, issues related to partial discharges phenomena are in principle less critical. However, there is a large difference at the design step as the electric field distribution is by far less controlled under DC than under AC stress. On the one hand, the resistivity, that drives the DC stress distribution in stationary conditions, is varying in a large extent with temperature, with field, and with the nature of material and is globally much less well controlled than the permittivity. On the other hand, charge accumulation may induce further field redistribution, and contributes to a large extent to the field value uncertainty, pointing to the need for materials limiting such charge accumulation. Finally, even under DC, capacitive field distributions are also effective, for example for some time after stress application and for all transient stresses applied to cables (surge, lightning, etc.). As will be shown in this work the passage from a capacitive to a resistive field distribution is relatively slow and we will focus on the behavior of the field in these transient conditions.

The computation results presented here utilize the empirical expressions for the field and temperature dependent electric conductivities, i.e. a macroscopic approach. Such models account for the gross trends regarding field distribution, allowing to predict so-called field inversion phenomena under DC stresses and field distribution in

multi-dielectrics. It is recognized, however, that such models are not capable of predicting the magnitudes of the maximum field stress and polarity of the accumulated space charges accurately [**3**] and the non-symmetrical behavior when changing voltage polarity [**4**]. More refined models based on bipolar charge transport (i.e., microscopic approach) in addition to the effects described by the macroscopic models, predict the experimentally observed accumulation of homo- and hetero-charge in the insulation reasonably well and provide convincing electric field estimations for HVDC cables. Such microscopic models are therefore preferable. However, correct identification and parameterization of the different processes at play is extremely tedious. The application of such model to cable joints is attempted [**5**], but there is still lot to be done for this parameterization combining differential insulating materials and possibly specific trapping behavior at the interfaces.

Temperature effects on the DC field distribution

In a cable energized under DC stress, the cylindrical geometry and the conductivity gradient associated with the thermal gradient within the insulation represent the main controlling factors for the field distribution. Besides the geometrical design and applied stresses, which are perfectly controlled, the main necessary input data on materials for computing the field distribution are the field and temperature dependencies of the electrical conductivity and the thermal conductivity.

The transient electric field in a cable under DC voltage can be calculated numerically resolving the following set of local equations in time-dependent conditions:

Gauss law: $$\nabla(\varepsilon \mathbf{E}) = \rho \tag{1}$$

Current continuity: $$\nabla(\mathbf{J}) = -\frac{\partial \rho}{\partial t} \tag{2}$$

Conduction: $$\mathbf{J} = \sigma \mathbf{E} \tag{3}$$

where **E** is the electric field vector, **J** is the conduction current density, ρ is the free charges density, ε is the permittivity of the insulation, σ is the material electrical conductivity.

The local equation governing the heat exchange is [**6**]:

Heat: $$\rho_m C_p \frac{\partial T}{\partial t} = \nabla(\lambda \nabla T) + S_{heat} \tag{4}$$

where ρ_m [g/m^3] is the mass density, C_p [J/g/K] is the specific heat capacity and λ [W/m/K] is the thermal conductivity. The term S_{heat} [W/m^3] represents the ohmic losses in the conductor and in the insulation materials.

The governing equation for temperature in a cylindrical geometry under steady state condition is the following:

Temperature: $$T(r) = T(r_r) + \frac{W_c}{2\pi\lambda} \ln \frac{r_r}{r} \tag{5}$$

where W_c is the heat produced per unit length of the conductor and λ is the thermal conductivity. The equation holds for any homogeneous layer, neglecting the heat produced by Joule losses in the insulation. The reference position r_r is taken at any position in the dielectric layer including the inner and outer radii. It is obvious here that the lower the thermal conductivity, the larger the temperature gradient across the insulation.

The electric field distribution is obtained simply by considering the conservation of the current through the insulation, i.e. from (3):

DC electric field: $$E(r) = E_r(r_r) \frac{r_r \sigma_r}{r \sigma(r)} \tag{6}$$

where E_r and σ_r are the electric field and the electrical conductivity, respectively, taken at the reference position r_r.

For the field under ac-stress, hypothesizing a radius-dependent permittivity, an equation similar to (6) is obtained based on the Gauss law (1) with no space charge:

AC electric field: $$\mathbf{E(r)} = \mathbf{E_r(r_r)}\frac{\mathbf{r_r \varepsilon_r}}{\mathbf{r\varepsilon(r)}} \quad (7)$$

Under homogeneous permittivity or conductivity conditions, with no space charges, and considering the limit condition with potential V applied to the cable conductor, (6) or (7) lead to the geometric field distribution:

Geometric electric field: $$\mathbf{E}_g\mathbf{(r)} = \frac{\mathbf{V}}{\mathbf{r} \cdot \mathbf{ln}(\mathbf{r_i}/\mathbf{r_o})} \quad (8)$$

Hence, when applying a DC stress, the field distribution evolves from a geometric one (at short time) to a resistive one described by (6). All the steps along the field redistribution under transient conditions are governed by the field and temperature dependency of the conductivity and by the thermal response of the energized cable.

The temperature profile is relatively easy to anticipate, depending on the limit conditions at the outer layer of the cable and on the construction of the cable (semiconductor, shield, outer sheath).

Therefore, the model adopted for the conductivity law is of real importance. A convenient way to model it consists in using an exponential law for both the field and temperature dependency of the conductivity:

Eoll's rule: $$\boldsymbol{\sigma_1(T,E)} = \boldsymbol{\sigma_r} \cdot \mathbf{exp}\ \boldsymbol{\alpha_T(T - T_r)} \cdot \mathbf{exp}\ \boldsymbol{\alpha_E(E - E_r)} \quad (9)$$

where $\boldsymbol{\alpha_T}$ and $\boldsymbol{\alpha_E}$ are temperature and field dependency coefficients, respectively. A great advantage of this approach is that it provides and analytical solution to the steady state field distribution in the cable under load condition [**7**], [**8**], [**9**]. Though empirical in nature, the model is well adopted for the case of impregnated paper insulation [**10**]. Pushed by application needs in standards, the natural trend is to extent this rule to the case of other kinds of insulations. Hampton [**8**] collected and ensemble of data for different kinds of polymeric insulations, including laminated insulation. The set was used to compare the DC field distributions obtained in these different insulations, showing the major effect of temperature dependence of the conductivity over the field dependence to control the field distribution. The use of an empirical equation as (9) can be admitted provided the description is closely representative of the material behavior. This seems the case, at least in the range of temperature variation inside cable insulation. However, when dealing with polymers, such an exponential dependence of the conductivity with temperature does not appear really justified, and activated process has been used instead [**11**].

Indeed, an expression for the conductivity using an Arrhenius-like dependence for the temperature dependence and "quasi-hyperbolic sine" on electric field can be more easily justified, accounting for thermally activated transport processes and for the shift from linear to non-linear field dependence of conductivity operating through a hoping or ionic conduction process [**12**], [**13**]:

$$\boldsymbol{\sigma_2(T,E)} = \boldsymbol{\sigma_r} \cdot \mathbf{exp}\frac{\mathbf{Ea}}{\boldsymbol{k}}\left(\frac{\mathbf{1}}{\mathbf{T_r}} - \frac{\mathbf{1}}{\boldsymbol{T}}\right) \cdot \frac{\boldsymbol{sh(\beta_E E)}}{\boldsymbol{\beta_E E}} \quad (10)$$

where **Ea** is the activation energy and $\boldsymbol{\beta_E}$ a field coefficient. As will be shown below, in the association of dielectrics, the exact field distribution depends directly on the ratio of conductivity in adjacent materials. Therefore, it is of even higher importance to have a clear estimation of the conductivities of materials used in accessories compared to single insulation as in cable core. In Eq (10), the field dependence of the conductivity is similar to that in (9) except for the linear variation at small field which is added. However, the temperature dependencies are substantially different. To compare the two relations, let consider the apparent activation energy for the conductivity following a power law (9):

$$\mathbf{Ea}_{\mathbf{1}\boldsymbol{app}} = -\frac{\boldsymbol{k}}{\boldsymbol{\sigma_1}}\frac{\mathbf{d}\boldsymbol{\sigma_1}}{\boldsymbol{dT^{-1}}} = \boldsymbol{k}\ \boldsymbol{\alpha_T}\mathbf{T^2} \quad (11)$$

Figure 1 shows an example of conductivity and apparent activation energy vs. temperature obtained on EPDM with a fit to (9) providing $\boldsymbol{\alpha_T}$ = 0.086 K^{-1} [**14**]. Here, the activation energy rises substantially with temperature, from 0.65 eV at 20°C to about 1.0 eV at 90°C, corresponding to the move from a 'good' to a 'bad' DC insulation according to Boggs' *et al* criteria [**15**].

The field distortion introduced by the conductivity gradient along the cable radius is associated to a space charge distribution. Combining (1), (3) and (5), the charge distribution in steady state condition is of the form:

$$\rho(\mathbf{r}) = -\mathbf{E}(\mathbf{r})\frac{\varepsilon}{\sigma(\mathbf{r})}\frac{\partial\sigma}{\partial\mathbf{r}} + \mathbf{E}(\mathbf{r})\frac{\partial\varepsilon}{\partial\mathbf{r}} \quad (12)$$

Supposing a negative charge is applied to the cable conductor and a temperature gradient produces a decreasing conductivity with the radius, then the field is negative and the contribution to space charge due to the conductivity gradient is negative. Hence, the electric field modulus is reduced near the conductor and increased near the outer screen compared to the geometric field distribution. This kind of space charge and induced field distribution should be detected using charge measurement techniques in the same way as space charges resulting from deep charge trapping into the insulation.

A negative space charge will also result if the permittivity decreases when approaching the interface on the conductor side, as for example if polar by-products are expelled through the dielectric surface. It is considered that the permittivity can be decreasing or increasing, as a result of inter-diffusion of polar groups [**16**] [**17**]. In a general way, the consequence of the presence of an excess of polar groups near the interface is an interface field reduction, and reciprocally, a loss in polar groups leads to interface field strengthening [**18**] [**19**]. If property gradient, whether it be permittivity or electrical conductivity, is at the origin of space charge, then, according to the macroscopic description given here, the charge profile should be perfectly symmetrical when changing the polarity of the applied voltage. This constitutes one criterion to discriminate between charge trapping and property gradient.

The field redistribution due to the presence of polar groups-containing region is driven by the same rules as that involving insulations of different nature. This is specifically the situation met in cable accessories where polymeric dielectrics of different nature coexist.

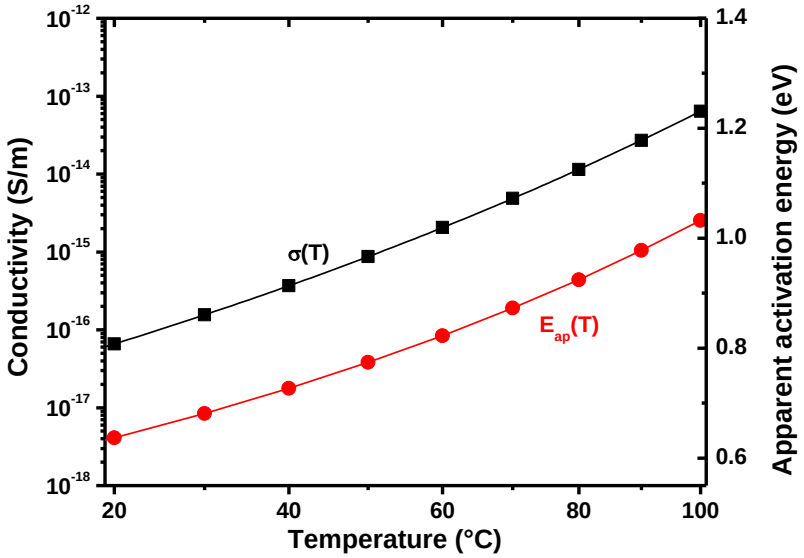

Figure 1 Arrhenius graph of the temperature dependence of the conductivity of EPDM following (9) with $\boldsymbol{\alpha_T}$ = 0.086 m/V, $\boldsymbol{\sigma_r}$ = 1.18 10^{-17} S/m for E = E_r = 0 and T_r = 0 °C. Corresponding apparent activation energy obtained from (11).

Field distribution in multi-dielectrics

Pre-molded cable accessories involve the association of cable insulation, most generally cross-linked polyethylene (XLPE), and of an elastomer that can be SiR, i.e. Silicone Rubber or EPDM, a terpolymer constituted of ethylene, propylene and diene monomer [**20**] [**21**]. Equations (1)-(3) still govern the field distribution when associating dielectrics of different nature. The space charge formed due to the permittivity and/or electrical conductivity gradient is an interface charge and the build-up of this charge is known as Maxwell-Wagner (MW) effect.

Considering the case of a flat geometry, when associating two dielectrics of different properties, the following set of equations holds in steady state conditions:

$$\boldsymbol{\sigma_1(E_1)\cdot E_1 = \sigma_2(E_2)\cdot E_2} \quad (13)$$

$$\boldsymbol{\varepsilon_2 \cdot E_2 = \varepsilon_1 \cdot E_1 + \Sigma_s} \quad (14)$$

$$\boldsymbol{d_1 \cdot E_1 + d_2 \cdot E_2 = -V_0} \quad (15)$$

where the dielectric (1) is for $0<x<d_1$, and dielectric (2) for $d_1<x<d_2$ and $V(0)=0$, $V(d_1+d_2)=V_0$. $\boldsymbol{\varepsilon_i}$ is the permittivity, $\boldsymbol{\sigma_i}$ is the field-dependent conductivity, and $\boldsymbol{\Sigma_s}$ is the interfacial charge. The equations describing the non-stationary regime are the same and they are obtained by incorporating the time dependence of the fields $\mathbf{E_1}$ and $\mathbf{E_2}$ and writing the interfacial charge density in the form [**22**] [**23**]:

$$\boldsymbol{\Sigma_s(t) = \frac{\varepsilon_1 \cdot \sigma_2(t) - \varepsilon_2 \cdot \sigma_1(t)}{d_1 \cdot \sigma_2(t) + d_2 \cdot \sigma_1(t)} \cdot V_0 \cdot \left(1 - e^{-t/\tau_{MW}(t)}\right)} \quad (16)$$

with:

$$\boldsymbol{\tau_{MW}(t) = \frac{\varepsilon_2 \cdot d_1 + \varepsilon_1 \cdot d_2}{d_1 \cdot \sigma_2(t) + d_2 \cdot \sigma_1(t)}} \quad (17)$$

Only in specific conditions of the ratios between permittivity and conductivity the interface charge is null: $\boldsymbol{\sigma_2/\sigma_1 = \varepsilon_1/\varepsilon_2}$. In the general case, a redistribution of the field occurs while the interface charge builds-up after a change in applied voltage. As the fields $\mathbf{E_1}$ and $\mathbf{E_2}$ vary with time during the redistribution of the interface charge, the conductivities $\boldsymbol{\sigma_1}$ and $\boldsymbol{\sigma_2}$ also depend on the time due to the non-linear behavior.

The predicted charge quantities according to (16) based on conductivity measurements are rather well verified when measuring space charge in flat bilayers, quantitatively and kinetically, considering charge build-up and decay [**24**]. In this simplified scheme however, charge trapping that may occur in the insulation is not taken into account. Different degrees of refinement of models for DC cables can be introduced, going from drift-diffusion models, to those involving conductivity gradients near the insulation interfaces (near electrodes or near inner interfaces between dielectrics) [**25**]. Introducing conductivity gradients will lead to space charge build-up. However, symmetric behavior of the field distribution when changing the polarity is predicted. It was shown that the interface charge can be modified by introducing specific trap properties near the material interfaces by appropriate treatment [**26**] [**27**]. In that case, differences in trapping for positive and negative charges can be introduced, and the macroscopic model, would it be with conductivity gradient, cannot explain the features. Recourse to drift-diffusion models is necessary, which are much more demanding in terms of computational resources.

A fundamental quantity in the above process is the charge relaxation time $\boldsymbol{\tau_{MW}}$. It may vary considerably as a function of time and temperature. To provide orders of magnitude, the variation is by 3 decades (≈2 min to 30 h), between 20 and 70°C and for fields up to 30 kV/mm when associating XLPE and EPDM [**23**].

Obviously, as will be shown below, in an accessory the field distribution will evolve in a more complex way, as the temperature is non homogeneous, and the geometry involves tangential contribution to the electric field. The resolution of the field distribution can no longer be achieved analytically as may be done for a cable due to the more complex geometry. For that, finite element modelling is used and the accuracy of the modelling is driven primarily by the correctness of conductivity data provided to the model. Several recent works treat modelling of the field distribution in joints, including the transient states [**5**] [**17**] [**28**]. Also, modelling can be used to determine optimal properties of materials for field homogenization, being insulations or field grading layers [**29**].

It remains that on the practical side, reliable data must be gathered regarding conductivity laws, which can be a tedious task. In addition, it is difficult to get a generic behavior for a particular kind of polymer. Table 1 provides a set of data relevant to the physical properties of XLPE, EPDM and SiR. The determination of electric conductivity versus field and temperature of XLPE and EPDM materials is reported elsewhere [**24**]. They gave consistent data when comparing measured and modelled field distributions in bilayers, assessing the correctness of the model at least at the sample scale. The used equation is:

$$\boldsymbol{\sigma_3(T,E) = A \cdot \exp\left(-\frac{Ea}{kT}\right) \cdot \frac{sh(\beta_E(T).E)}{E^a}} \quad (18)$$

It accounts for the non-linear behavior at low field and for the fact that the threshold field for the change in conduction regime decreases with temperature, through a temperature dependent $\boldsymbol{\beta_E}$coefficient.

For the silicone rubber, we used, for the simulations presented in the following, the expression of conductivity given by Baferani *et al* [**30**], corresponding to Eq (9). Compared to EPDM, SiR shows a higher electrical permittivity, a

lower thermal conductivity and much less variation of conductivity vs. temperature and electric field. With a temperature coefficient of 0.019 K^{-1}, the equivalent activation energy deduced from (11) is of 0.15 to 0.18 eV in the temperature range 30-60°C, which is considerably lower than that of EPDM or XLPE.

Table 1. Thermal and electrical parameters for various materials.

	XLPE	**EPDM**	**SiR**	**Semicon**
Relative permittivity ε_r	ε_r = 2.30	ε_r = 2.90	ε_r = 3.50	ε_r = 2.30
Thermal conductivity	λ = 0.38 W/m/K	λ = 0.30 W/m/K	λ = 0.20 W/m/K	λ = 0.34 W/m/K
Specific heat	c_p = 1.90 J/g/K	c_p = 0.73 J/g/K	c_p = 2.25 J/g/K	c_p = 1.90 J/g/K
Electrical conductivity	Eq (18)	Eq (18)	Eq (9)	Constant
σ (30 °C, 2 kV/mm)	4.7×10^{-17} S/m	1.0×10^{-15} S/m	9.2×10^{-15} S/m	6.0×10^{3} S/m
Temperature coefficient	E_a = 1.0 eV	E_a = 0.44 eV	α_T =0.019 K^{-1}	
Field coefficient /30 °C Field coefficient /60 °C	β_E =1.38 × 10^{-7} m/V β_E =1.12 × 10^{-7} m/V	β_E =0.95 × 10^{-7} m/V β_E =1.08 × 10^{-7} m/V	β_E =4.1 × 10^{-16} m/V	
Field power law	a = -0.15	a = 1.42	---	

Figure 2 shows a comparison of conductivity as a function of the field for the different materials at different temperatures. Comparing XLPE and EPDM, the conductivity is sometimes higher in one material or the other, depending on the field and temperature conditions, which will result in a transfer of the DC field in one or the other of the materials according to these same conditions.

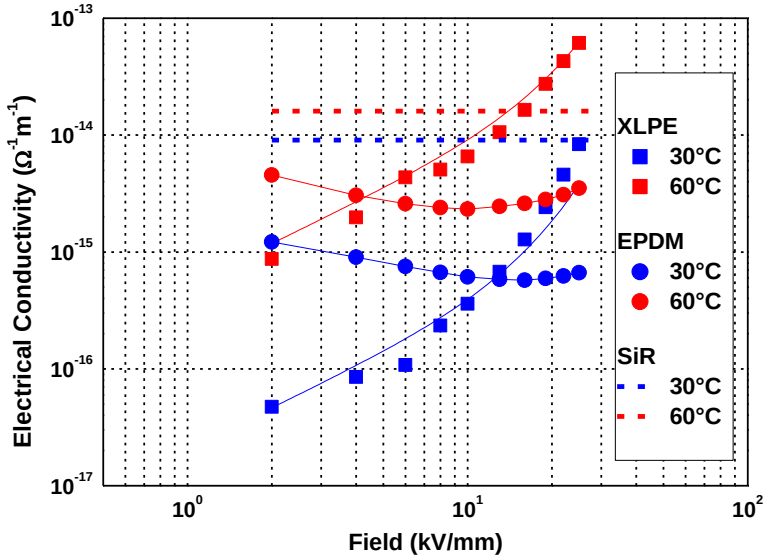

Figure 2. Field dependence of the electrical conductivity of XLPE, EPDM and SiR at 30 and 60°C.

Not many reports on DC conductivity measurements using reasonable charging time are available in the literature for EPDM. A quasi field-independent conductivity of EPDM for fields up to 10 to 20 kV/mm was reported, contrasting with the strong field dependence of conductivity of XLPE [**31**]. Besides, EPDM is a complex material, and its behavior may change with compounding: D. Li *et al* [**32**] found power law relation between conductivity and field with an exponent in the range from 0.2 to 0.9, depending on EPDM grade (with using only 1 min charging time!).

Figure 2 reveals an apparent decrease of the conductivity of EPDM with the field (at up to 10kV/mm) which is rather appealing. The behavior was explained by possible contribution from ionic conduction as happens in liquids [24]. Recently, Mourad *et al* reported on a similar observation in the case of SiR insulation [**14**]. The corresponding data are plotted in Figure 3. The decrease of conductivity with the field observed for SiR was explained by charge injection and trapping that limit the field at the electrode. Conductivity data were fitted using (9). For field lower than the threshold for charge injection (≈ 18 kV/mm), the reported temperature coefficients are $\boldsymbol{\alpha_T}$ = 0.04 and 0.086 K^{-1} for SiR and EPDM respectively and the field coefficients are $\boldsymbol{\beta_E}$ = -1.4 × 10^{-7} and 1.1 × 10^{-7} m/V. Qin *et al* [**33**] also used an expression as (18) with $\boldsymbol{\beta_E}$ =5.43 × 10^{-8} m/V (a = 1) providing a mild field dependence of the

conductivity in SiR. However, the activation energy is 0.72 eV, which is relatively large. Häring and Jenau [**34**] reported on similar results, with an activation energy of about 0.71 eV and $\beta_E \approx 1.0 \times 10^{-7}$ m/V (at 30°C, rising with temperature) on two different silicone rubbers.

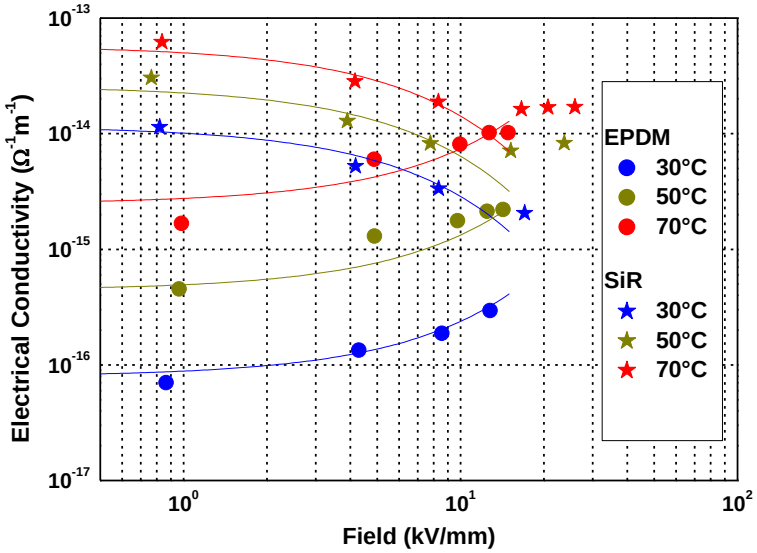

Figure 3. Field dependence of the electrical conductivity of EPDM and SiR at 30, 50 and 70°C from [14].
Lines are fit to Eq (9) in the low field range: For EPDM, $\boldsymbol{\alpha_T}$ = 0.086 K^{-1} and $\boldsymbol{\beta_E}$ =1.1 × 10^{-7} m/V; for SiR $\boldsymbol{\alpha_T}$ = 0.04 K^{-1} and $\boldsymbol{\beta_E}$ = -1.4 × 10^{-7} m/V.

The conclusion about these various reports on conductivity data on joint materials is that the real conduction function can be extremely variable depending on material source or compounding, possibly also on the way measurements are carried out. The material used as joint, EPDM to cite an example, contains a great amount of fillers, also oil, in such a way that the EPDM polymer may represent less than 50% by weight [**35**]. The span in electrical conductivity is considerable and it can therefore be anticipated that the electric field distribution in situations involving temperature gradients, geometry singularities and materials association can be only approximately anticipated.

Field modelling in 200kV joint model in transient state

Figure 4 provides a cross-section of the joint model used in the present simulations. Details of the joint construction and limit conditions are given elsewhere [**28**]. The field distributions were computed considering 3 associations of materials: XLPE/EPDM, XLPE/SiR and XLPE/XLPE, the latter being representative of an interface-free joint. To account for the field distribution, profiles along direction (1) were considered, and focus is given on the tangential field variation along direction (2), as it represents a weak point of the joint. The data listed in Table 1 have been used to determine the electric field distributions in the joint submitted to a DC voltage of +/-200kV. The heat input by the Joule effect in the copper conductor takes into account a reference resistivity of 1.7 × 10^{-8} Ω.m for copper at 20 °C and a temperature coefficient for the resistivity of 3.9 × 10^{-3} K^{-1}. The initial thermal condition was isothermal (at 30°C). The current of 1 kA is injected in the conductor of section 50 mm² at the same time as the voltage is applied. Then the field redistributes due both to thermal evolution and to achievement of a resistive distribution. We also show the results when the current is not injected and only the field is applied.

Critical regions for the electric field are under the cones at the ends of the joint and near the central deflector. Note here that more refined geometries can be defined, notably large notches can be designed at the ends of the deflector [**6**] [**30**] [**36**].

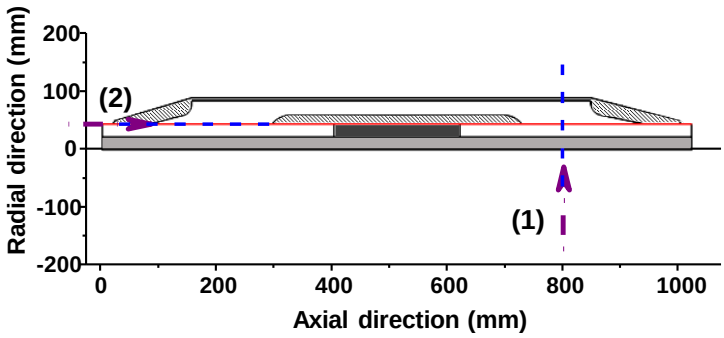

Figure 4. Scheme of the joint. (1) and (2) define cuts along which tangential field and radial field are represented in the following. White area: insulations (XLPE and joint material); Hached area: semicon; Light grey: conductor and soldering; dark grey: heat distributor.

As is shown in Table 1, the thermal conductivity of SiR is lower than the one of XLPE or EPDM. As a consequence, the thermal gradient is not the same for the different couples. The thermal conductivity of the material has a significant impact on the temperature distribution in this design of the joint. Figure 5 shows the steady state temperature profiles along direction (1) of Figure 4, for the three materials. Because of a lower thermal conductivity, the temperature near the conductor is nearly 10°C higher with SiR joint material than with a full-XLPE joint. The inset shows the transient temperature at the dielectric/dielectric interface. The temperature takes over 24 h to be equilibrated in case of SiR. The slower temperature rise is explained by the thermal time constant, which by analogy with electrical conductivity is related to the ratio between specific heat and thermal conductivity: c_p / λ, which is much larger in case of SiR, see Table 1. This slow time constant in the system shows that probably in real situation the temperature is continuously redistributing due to fluctuations in the transmitted power.

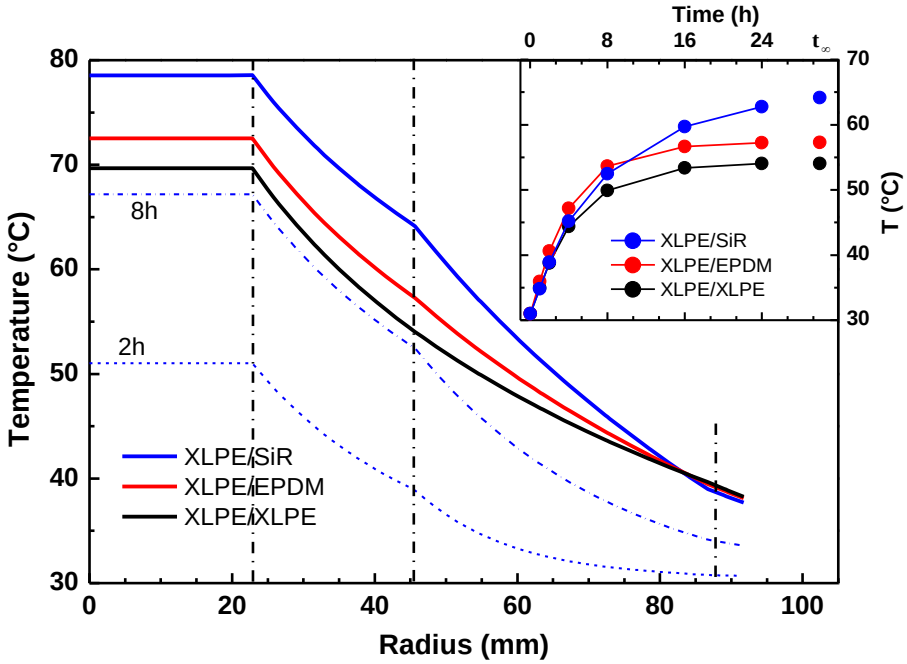

Figure 5. Radial temperature profiles in steady state (24 h) for the three material couples considered and profiles during thermal transient for XLPE/SiR at 2 h and 8 h (dashed lines). In inset: temperature rise at the interface between XLPE and joint material.

Maps of the potential and field are represented in Figure 6, considering different times: a) just after positive voltage application, representing essentially the capacitive field distribution, then b) just after polarity reversal after stressing for 24 h under positive voltage and c) after 24 h under negative voltage. The differences in Fig. 6a) are due only to the permittivity differences for the joint material. The consequence is a move of the field to the cable insulation as the permittivity of the joint material is increased, going from XLPE, to EPDM and to SiR. Just after polarity reversal, Fig. 6.b), the radial component of the field appears much larger in the XLPE layer.

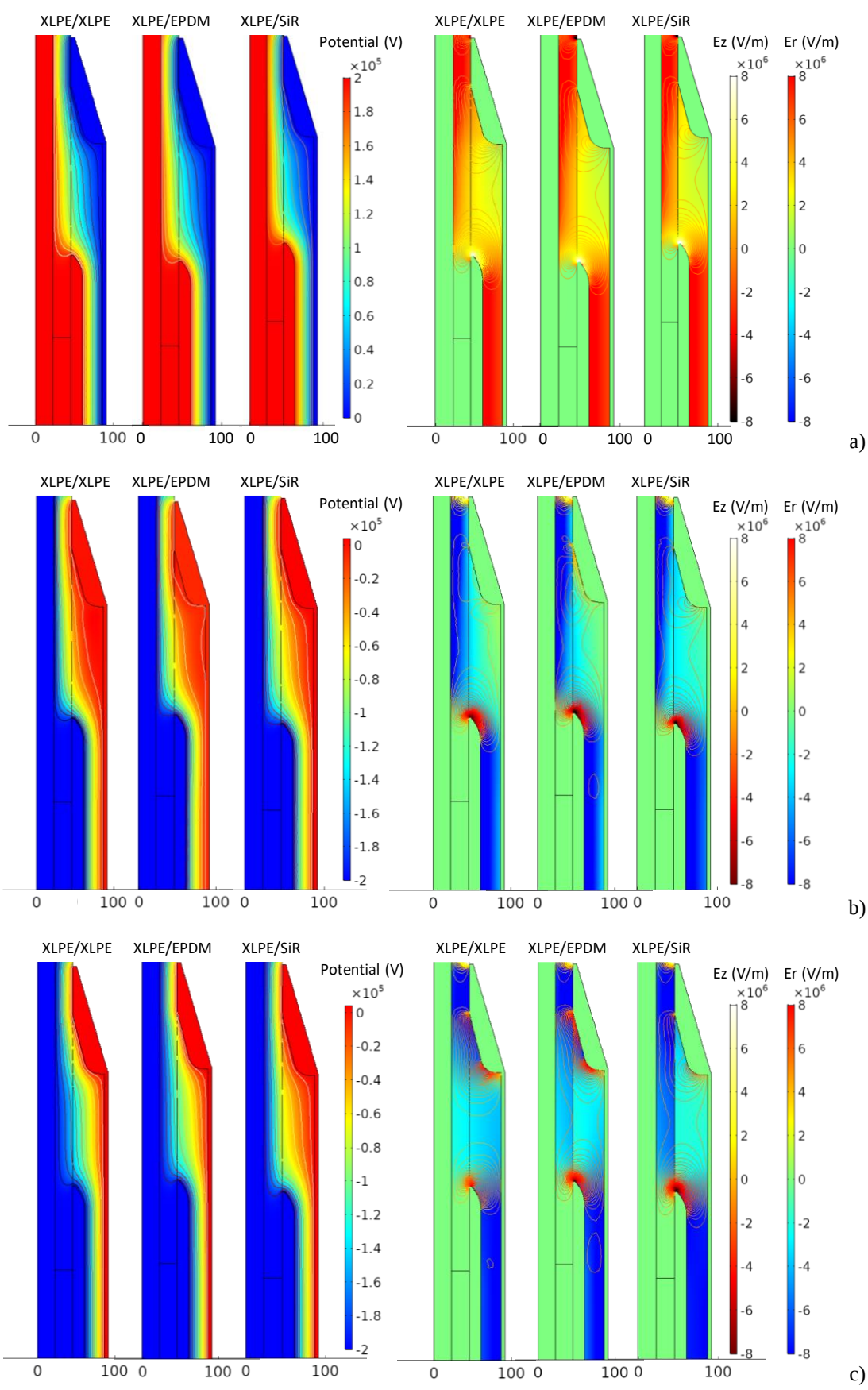

Figure 6. Left: Potential distribution; **Right:** Radial (surface, Er) and tangential (contour lines, Ez) field distributions for XLPE/XLPE, XLPE/EPDM and XLPE/SiR joints at selected times: **a)** 3' after +200 kV voltage application; **b)** 3' after voltage inversion to -200 kV and **c)** 24 h under -200 kV. The initial temperature is 30 °C and current is injected in the conductor.

The field results from the residual field built during the switch from capacitive to resistive distribution during the positive voltage application and the capacitive field resulting from negative voltage application. The resulting field under the cone is weak for the XLPE/XLPE joint; it is slightly positive with the EPDM joint material and negative for the SiR material. In Fig. 6c), the results are representative of the field distribution in steady state under thermal gradient. The field under the cone is decreasing when going from XLPE, to EPDM and to SiR, and is growing near the central deflector.

The field variations change a lot with joint insulation material, Fig. 7b. For SiR joint (green color), the field at the inner interface rises in the first hour and then decreases, as the temperature rise acts against the conductivity gradient in the joint. The stress inversion in the cable insulation occurs after 4 h (the field at the inner interface of cable insulation becomes less than that at the outer interface). The full-XLPE joint material is the one showing the most homogenous field. The stress inversion occurs with small final differences in field values along the thickness. The peak in field at the polarity reversal is nearly as large for SiR joint as for EPDM joint. The field redistribution with SiR is particularly fast after polarity reversal because of the high temperature in XLPE and high conductivity in SiR.

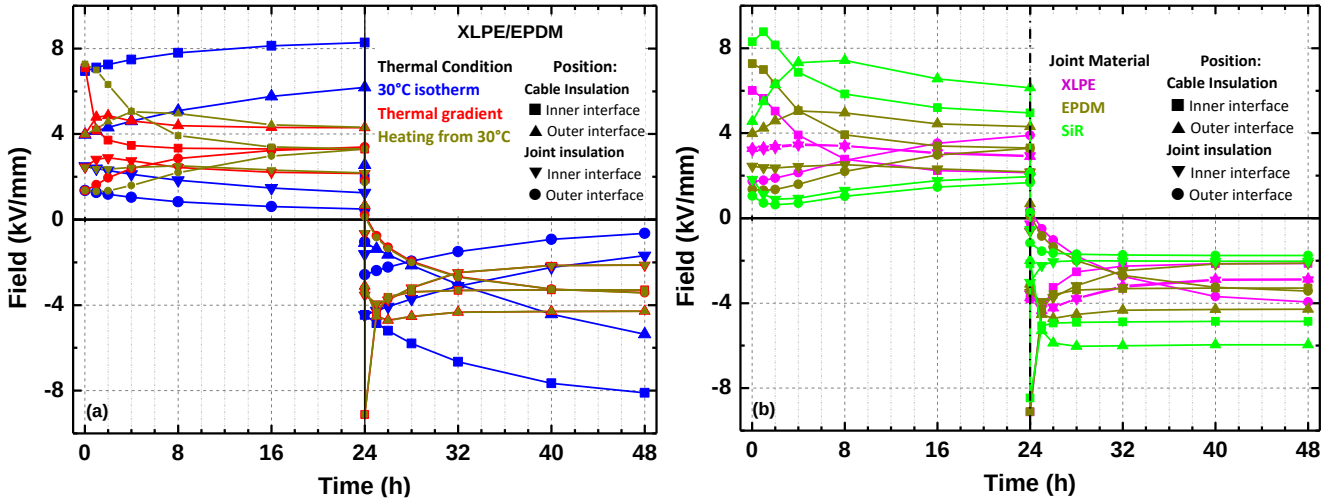

Figure 7. Radial variation of the electric field as a function of time under DC voltage of +200 kV followed by inversion to -200 kV after 24 h.
(a) XLPE/EPDM joint with different thermal conditions; (b) Different joint materials under non-stationary thermal gradient. The field is taken at 4 positions near the interfaces along direction (1) of Fig. 4.

As viewed in Figure 6, the tangential electric field along the interface between cable and joint insulation is strengthened under the cone and near the deflector. The distributions of the field are not the same for the different materials, being more spread in case of full-XLPE joint (Fig. 6c). Depending on conditions, the tangential field is balanced differently between the cone and deflector regions. Figure 8 shows the time dependence of the tangential electric field along the interface (cutline (2) in Fig. 4), considering the maximum value under the cone and near the deflector. As previously, cases of different thermal conditions (with EPDM joint material, Fig 8a) and different joint materials (Fig. 8b) are considered.

The circulation of the field being conservative, it can be stated that, along a line parallel to the axis of the joint:

$$\int_c^d \mathbf{E}_z \, dz = \mathbf{V}_c - \mathbf{V}_d \tag{19}$$

where $\boldsymbol{c}$ represents the deflecting cone and $\boldsymbol{d}$ the central deflector. Therefore, a field increase in a region is compensated by a decrease elsewhere along the interface, and the integral under the tangential field component is null during the grounding step.

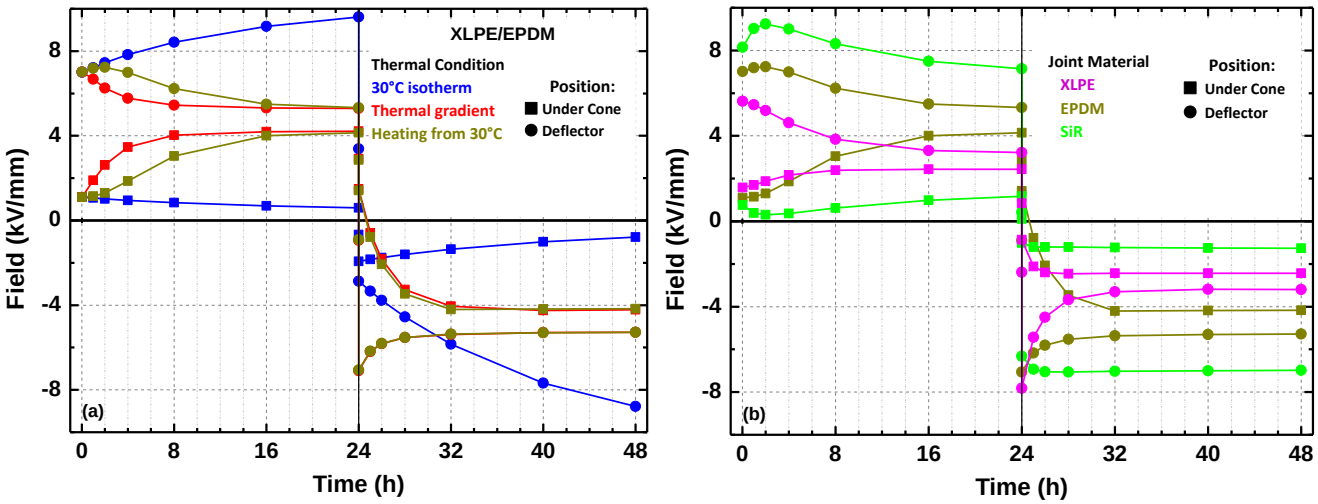

Figure 8. Variation of the tangential electric field at the dielectric/dielectric interface as a function of time under DC voltage of +200 kV followed by inversion to -200 kV after 24 h. (a) XLPE/EPDM joint with different thermal conditions; (b) Different joint materials under non-stationary thermal gradient. The maximum field under the cone and near the deflector are plotted.

For EPDM in isothermal conditions (Fig. 8a), the tangential field is significantly greater in the deflector region. This can be explained by a geometry that does not include a field-grading cone, unlike the potential reference side of the joint. Over time, the tangential field tends to decrease on the ground side and to strengthen significantly on the HV side. These trends reflect the non-linear nature of the conductivity as well as the conductivity gradient due to the presence of two insulators. In thermal gradient condition, the field increases over time on the cone side, by a factor 3. As a result, in the first moments of the polarity reversal, the sign of the field is not reversed. On the HV side, the field variations are milder. The negative residual field appearing at grounding is added to the applied field after inversion, and therefore produces an over-stress. Globally, the values of tangential fields remain lower than in the isothermal case. This is not necessarily an effect of the thermal gradient but of the fact that, taking into account the average applied stresses, the conductivity values of the two insulators become closer by heating the junction. They are identical at 60 °C for a field of 4 kV/mm, while at 30 °C the equivalence is obtained under a field of 15 kV/mm (Fig. 2) which is never reached here.

Using a single material, XLPE, under thermal gradient, the evolution of the field distribution is similar to the one with XLPE/EPDM in the same conditions (Fig. 8b). With the SiR joint material (Fig. 8b) having a much larger conductivity than XLPE, there is practically no field distortion on the ground side (the residual field at voltage removal is nearly zero) and the field is small compared to other cases. On the HV side, there is also a mild variation of the field with time, and hence weak residual field at grounding. Here the field reaches the highest values at about 7.5 kV/mm in steady state. The profiles are in fact similar to the ones for XLPE/EPDM at 30°C: the common feature here is a higher conductivity in the joint material than in cable insulation.

Besides conductivity differences, the temperature distribution may affect the axial field distribution. In steady state, the temperature on the deflector side is homogeneous in the axial direction. It is about 64°C for SiR joint and 57°C for EPDM. On the cone side, the temperature being minimum at the tip of the cone. A thermal gradient is set, spreading over ≈100 mm: it is about 3°C in case of EPDM joint and 7°C in case of SiR joint [**28**]. The effect of this thermal gradient could be to concentrate the field at the tip of the cone; however, this effect is not obvious in the results.

According to the results presented here, in order to obtain an equilibrated tangential field distribution along the interface, the electrical conductivities of the two insulations should be close. Conductivities should remain close in large range of temperature and electric field, since the thermal and electrical stresses are not homogeneous in the joint and vary with time. However, we have seen in the measurements that only in particular combinations (field-temperature), equal values of conductivity are obtained. It is in fact difficult to have similar behaviors in a broad temperature range in materials so different as silicones or EPDM and XLPE. In addition, to accommodate fast varying stresses, the ratio of electrical conductivities between the two materials should be the same as the ratio of permittivities. Then, no interface charge would build-up and the radial field redistribution at polarity reversals would be less, as seen in Fig. 7b for all-XLPE case. However, this is not confirmed on the tangential contribution which reaches 8kV/mm just after polarity reversal (Fig. 8b).

Using a joint material with relatively high electrical conductivity is an option for minimizing the field under the stress cone, moving it to the cable insulation and lowering the tangential field. This goes with field enhancement at the deflector side with the investigated geometry. Choosing a more suited design for the deflector could help to reduce the field. Regarding the high tangential field near the deflector for SiR joint, it would be interesting to check how far the thermal conductivity and the permittivity of SiR contribute to the difference with other cases. In general, the stresses at a given position evolve monotonously as a function of time in these non-stationary electrical and thermal conditions. However, there are cases where the maximum stress is obtained a few hours during stressing. For example, for SiR the peak in tangential and radial field is after 2h. Investigating in some details the transient conditions of field arrangement as done in the present work is really worth when often only a direct resolution in stationary state is proposed combined with geometric field distribution for the impulse stresses.

In another respect, to simplify the problem of the field distribution in the joint, a field grading layer can be inserted between the two dielectrics and cover the inner deflector or the metallic connector [**37**]. The role of the layer is to distribute the potential along the axial direction and to smooth field enhancement at the edges. An advantage is to decouple the stresses in the two insulations, providing field distributions independent from the behavior of the other material [**38**]. The development of such materials for obtaining the optimum non-linear characteristics is a topic in itself [**39**]. In cable domain, field grading materials are polymers filled essentially with SiC or ZnO and the conductivity is tuned by acting on the filler size distribution and ratio. Issues are with compounding, avoiding ageing of the material and treating the two interfaces created with the insulations with lubricants. Materials as silicone with non-linear properties to be used as joint insulation [**40**] could be an alternative to the setting of an extra layer. The development of HVDC cables with extra-high voltages and the requirement of extremely low failure rate on very long submarine and land cable links will certainly call for intense research in the design of accessories.

Conclusion

The field distribution in HVDC cable joints has been investigated in non-stationary electrical and thermal conditions, considering XLPE as cable insulation and different materials as joint insulation. The radial distribution of the field follows expected trends with temperature, depending on materials electrical conductivity. Regarding the tangential field distribution at the interface between joint and cable insulations, it is lower under the deflecting cone side when the electrical conductivity in the joint material is high. It results from a migration of the field into the cable insulation and to a reduction of the tangential component by geometrical factor. As a consequence, there is an increase of the tangential field towards the deflector side. The changes from one situation to another can be due to the nature of the material and to the thermal conditions.

The exact field distribution can be variable in a large extent as a function of thermal and electrical material properties and of thermal and electrical stresses: operation in transient stresses necessarily impacts the stress distribution. Multiple stress conditions can be tested by modelling. This is quite easily achievable, but it is important to stress that the collection of experimental data on conductivity, representative of materials in operating conditions, is a major preliminary step in all these modelling and design tasks. We have shown that the reported characteristics on materials can be extremely variable and hence the knowledge and mastering of thermal and electrical properties of candidate insulating materials is a prerequisite for pretending optimizing joints design.

Acknowledgment

This work is supported by CNRS International Scientific Cooperation Program (PICS) N° PICS07965.

References

[1] G. Mazzanti, "Issues and challenges for HVDC extruded cable systems," Energies, vol. 14, p. 4504 (pp. 1-34), 2021.

[2] Imdadullah, B. Alamri, M.A. Hossain and M.S.J. Asghar, "Electric power network interconnection: A review on current status, future prospects and research direction," Electronics, vol. 10, 2179 (29pp), 2021.

[3] S. Kumara, Y.V. Serdyuk and M. Jeroense, "Calculation of electric fields in HVDC cables: Comparison of different models," IEEE Trans. Dielectr. Electr. Insul., vol. 28, pp. 1070-1078, 2021.

[4] T. Takada, T. Tohmine, Y. Tanaka and J. Li, "Space charge accumulation in double-layer dielectric systems—measurement methods and quantum chemical calculations," IEEE Electrical Insulation Magazine, vol. 35, no. 5, pp. 36-46, 2019.

[5] Y. Wang, Y. Wang, X. Yang, A. Ma, Y. Sun and Y. Yin, "Charge transport in full-size HVDC cable joint with modeling of XLPE/EPDM interface," IEEE Trans. Dielectr. Electr. Insul., vol. 28, pp. 2117-2125, 2021.

[6] H. Ye et al., "Design aspects on HVDC cable joints," Proc. 12th International Conference on the Properties and Applications of Dielectric Materials (ICPADM), 2018, pp. 300-304.

[7] C. K. Eoll, "Theory of Stress Distribution in Insulation of HV DC Cables: Part I", IEEE Trans. Electr. Insul., vol. 10, pp. 27-35, 1975.

[8] R.N. Hampton, "Some of the considerations for materials operating under high-voltage, direct-current stresses," IEEE IEEE Electrical Insulation Magazine, vol. 24, no. 1, pp. 5–13, 2008.

[9] B. Diban and G. Mazzanti, "The effect of temperature and stress coefficients of electrical conductivity on the life of HVDC extruded cable insulation subjected to type test conditions," IEEE Trans. Dielectr. Electr. Insul., vol. 27, pp. 1313-1321, 2020.

[10] M.J.P. Jeroense and P.H.F. Morshuis, "Electric fields in HVDC paper-insulated cables," IEEE Trans. Dielectr. Electr. Insul., vol. 5, pp. 225-236, 1998.

[11] U. Nilsson, A. Campus, R.N. Hampton, M. Bergkvist, A. Farkas and M. Jeronse, "Material solutions for extruded HVDC cables," Proc. Jicable, Paper C.10.1.2, 2003, pp. 753–758.

[12] B. Diban, G. Mazzanti, N. Guerrini and I. Troia, "Deeper insight into the relationship between experimental expressions of conductivity and DC electric field in cables," Proc. 2021 IEEE Electrical Insulation Conference (EIC), 2021, pp. 437-440.

[13] N. Adi, T.T.N. Vu, G. Teyssèdre, F. Baudoin and N. Sinisuka, "DC model cable under polarity inversion and thermal gradient: build-up of design-related space charge," Technologies, vol. 5, 46 (16pp), 2017.

[14] M. Mourad, S. Haller, S. Iglesias and M. Henriksen, "Study of the electrical properties of HVAC EPDM and HVAC silicone rubber under DC constraint," Proc International Symp. on HVDC Cable Systems (Jicable-HVDC'21), 2021, pp. 1-6.

[15] S. Boggs, D. H. Damon, J. Hjerrild, J. T. Holboll and M. Henriksen, "Effect of insulation properties on the field grading of solid dielectric DC cable," IEEE Trans. Power Del., vol. 16, pp. 456-461, 2001.

[16] J. Hjerrild, J. Holboll, M. Henriksen, et al.: "Effect of semicon-dielectric interface on conductivity and electric field distribution," IEEE Trans. Dielectr. Electr. Insul., vol. 9, pp. 596–603, 2002.

[17] C. Jörgens and M. Clemens, "Conductivity-based model for the simulation of homocharges and heterocharges in XLPE high-voltage direct current cable insulation," IET Sci. Meas. Technol., vol. 13, pp. 975-983, 2019.

[18] F.N. Lim, R.J. Fleming and R.D. Naybour, "Space charge accumulation in power cable XLPE insulation," IEEE Trans. Dielectr. Electr. Insul. vol. 6, pp. 273-281, 1999.

[19] B. Vissouvanadin, S. Le Roy, G. Teyssedre, C. Laurent, I. Denizet, M. Mammeri and B. Poisson, "Impact of concentration gradient of polarizable species on the electric field distribution in polymeric insulating material for HVDC cable," IEEE Trans. Dielectr. Electr. Insul., vol. 18, pp. 833-839, 2011.

[20] M. van Duin, N. van der Aar and G. van Dornemaele, "Defining EPDM for the past and the next 50 yearsn" Kautschuk Gummi. Kunststoffe 70, pp. 14-23, Dec 2017.

[21] G. Mazzanti, J. Castellon, G. Chen, J. Fothergill, M. Fu, N. Hozumi, J.H. Lee, J. Li, M. Marzinotto and F. Mauseth, "The insulation of HVDC extruded cable system joints. Part 1: Review of materials, design and testing procedures," IEEE Trans. Dielectr. Electr. Insul., vol. 26, pp. 964–972, 2019.

[22] P.H.F. Morshuis, R. Bodega, D. Fabiani, G.C. Montanari, L.A. Dissado and J.J. Smit, "Dielectric interfaces in DC constructions: Space charge and polarization phenomena," Proc. IEEE International Conference on Solid Dielectrics (ICSD), 2007, pp. 450–453.

[23] T.T.N. Vu, G. Teyssedre, S. Le Roy and C. Laurent, "Maxwell-Wagner effect in multi-layered dielectrics: interfacial charge measurement and modelling," Technologies, vol. 5, 27 (15pp), 2017.

[24] T.T.N. Vu, G. Teyssedre, B. Vissouvanadin, S. Le Roy and C. Laurent, "Correlating conductivity and space charge measurements in multi-dielectrics under various electrical and thermal stresses," IEEE Trans. Dielectr. Electr. Insul., vol. 22, pp. 117-127, 2015.

[25] C. Jörgens and M. Clemens, "A review about the modeling and simulation of electro-quasistatic fields in HVDC cable systems", Energies, vol. 13, 5189 (42pp), 2020.

[26] J. Li, B. X. Du and H. Xu, "Suppressing interface charge between LDPE and EPDM for HVDC cable accessory insulation," IEEE Trans. Dielectr. Electr. Insul., vol. 24, pp. 1331-1339, 2017.

[27] Z.H. Zhang et al., "Mechanism and suppressing method of interface charge accumulation in HVDC cable accessory," Proc. 2020 IEEE 3rd International Conference on Dielectrics (ICD), 2020, pp. 550-553.

[28] T.T.N. Vu, G. Teyssedre and S. Le Roy, "Electric field distribution in HVDC cable joint in non-stationary conditions," Energies, vol. 14, 5401 (17pp), 2021.

[29] Y. Späck-Leigsnering, G. Ruppert, E. Gjonaj, H. De Gersem and M. Koch, "Towards electrothermal optimization of a HVDC cable joint based on field simulation," Energies, vol. 14, 2848 (13pp), 2021.

[30] M. A. Baferani, T. Shahsavarian, C. Li, M. Tefferi, I. Jovanovic and Y. Cao, "Electric field tailoring in HVDC cable joints utilizing electro-thermal simulation: effect of field grading materials," Proc. 2020 IEEE Electrical Insulation Conference (EIC), 2020, pp. 400-404.

[31] Z.Y. Li, W.F. Sun and H. Zhao, "Significantly improved electrical properties of photo-initiated auxiliary crosslinking EPDM used for cable termination," Polymers, vol. 11, 2083 (11pp), 2019.

[32] D. Li, Z. Zhu, L. Yang and Y. Ma, "Research on nonlinear EPDM for ± 525 kV HVDC Cable Accessories," MATEC Web Conf., vol. 260, 02001 (5pp), 2019.

[33] Y. Qin, N. Shang, M. Chi and X. Wang, "Impacts of temperature on the distribution of electric-field in HVDC cable joint," Proc. 2015 IEEE 11th International Conference on the Properties and Applications of Dielectric Materials (ICPADM), 2015, pp. 224–227.

[34] D. Häring and F. Jenau, "Apparent DC conductivity of silicone rubber compounds," Proc. 2020 IEEE 3rd International Conference on Dielectrics (ICD), 2020, pp. 1-5.

[35] C. Canaud, M. Antonio Sens, L.L. Yuan Visconte and R.C. Reis Nunes, "EPDM formulations for electric wires and cables," Kautschuk Gummi. Kunststoffe 54, pp. 56-30, Jan 2001.

[36] S.J. Frobin, C.F. Niedik, C. Freye, F. Jenau, D. Häring and G. Schröder, "A Generic approach for HVDC cable accessories modelling," Proc. 2018 IEEE 2nd International Conference on Dielectrics (ICD), 2018, pp. 1-6.

[37] A. Gustafsson, M. Jeroense, P. Sunnegårdh, M. Saltzer, H. Ghorbani and H. Rapp, "New developments within the area of extruded HVDC cables," Proc. 11th IET International Conference on AC and DC Power Transmission, 2015, pp. 1-5.

[38] H. Ghorbani, M. Jeroense, C. Olsson and M. Saltzer, "HVDC cable systems—Highlighting extruded technology," IEEE Trans. Power Delivery, vol. 29, pp. 414-421, 2014.

[39] A. Can-Ortiz, L. Laudebat, Z. Valdez-Nava and S. Diaham, "Nonlinear electrical conduction in polymer composites for field grading in High-Voltage applications: A review," Polymers, vol. 13, 1370 (58pp), 2021.

[40] S. Hou, M. Fu, C. Li, B. Han, C. Zhang and Z. Li, "Electric field calculation and analysis of HVDC cable joints with nonlinear materials," Proc. 2015 IEEE 11th International Conference on the Properties and Applications of Dielectric Materials (ICPADM), 2015, pp. 184-187.